41st Aerospace Sciences Meeting and Exhibit
6-9 January 2003, Reno, Nevada

AIAA 2003-545

Wind Thermochemical Models and Recent Improvements*

D. W. Lankford†
Jacobs Sverdrup AEDC Group
Arnold Engineering Development Center
Arnold Air Force Base, TN 37389

Mori Mani‡
The Boeing Company
St. Louis, MO 63166

Abstract

The thermochemical and transport models contained in the Wind computational fluid dynamic (CFD) code have been modified and extended over the last several years. This paper documents these updates; included are improvements to thermodynamics models, the addition of an effective binary diffusion model, and improved numerical solution of the chemical source terms. Implementation of the newest NASA thermodynamic curve fits is described including computation of multicomponent properties derived from these functions. Computation of transport properties from the Lennard-Jones parameters and the subsequent computation of the multicomponent effective binary diffusion coefficient are presented. Implementation of the parasol method for solving the species conservation equations with chemical source terms is described. Species-dependent, third-body efficiency that previously has been available in only one reaction model has been included in all the reaction models. The influence of third-body efficiency is investigated for supersonic reacting flow over a Mach 4.0 wedge. Computational results comparing the effective binary diffusion model and the Wilke model are presented.

Nomenclature

$a_{1\text{-}8}$	Thermodynamic curve fit coefficients
b_1, b_2	Thermodynamic curve fit coefficients
C_b, C_f	Backward, forward rate coefficients
$\vec{C}$	Vector of molar concentrations
C_p^0	Heat capacity at constant pressure
D_b, D_f	Backward, forward activation energy
D	Diffusivity
E^0	Molecular internal energy
$E_{r,s}$	Reaction (r), third body (s), efficiency
ΔG_γ	Gibbs function for complete reaction
g	Gibbs free energy
H^0	Enthalpy
K	Equilibrium constant
k	Thermal conductivity
$k_{f,r}$	Reaction (r), forward rate
$k_{b,r}$	Reaction( )r, backward rate
L_e	Lewis number
M_s	Third-body molecule
M_i	molecular weight of species I
Pr	Prandtl number
p	Pressure
R	Universal gas constant
r	Distance between molecules
S_b	Backward rate temperature exponent
S_f	Forward rate temperature exponent
S^0	Entropy
$S_{1\text{-}4}$	Molecular species
T	Temperature
β	Ratio of enthalpy to internal energy
$\hat{\beta}$	"Effective gamma"
γ	Ratio of specific heats

* The research reported herein was performed by the Arnold Engineering Development Center (AEDC), Air Force Materiel Command. Work and analysis for this research were performed by personnel of The Boeing Company and by personnel of Jacobs Sverdrup AEDC Group, technical services contractor for AEDC. Further reproduction is authorized to satisfy needs of the U. S. Government.

† Senior Member, AIAA.

‡ Associate Fellow, AIAA.

κ	Boltzmann's Constant
μ	Viscosity
υ'_i	Reactant i stoichiometric coefficient
υ''_i	Product i stoichiometric coefficient
ξ	Number of degrees of freedom
ξ_{ij}	Molecules i,j attractive energy
ρ	Density
σ	Collision diameter
ϕ_{ij}	intercollision parameter
χ_i	Mole fraction of species i
$[\chi_i]$	Molar concentration of species i
$\dot{\omega}_s$	Molar production rate of species s
$\Omega_{D,ij}$	Nondimensional collision integral

Superscripts

0	Standard state

Subscripts

b, f	Backward, forward
i, j, s	Specie index
r	Reaction index
mix	Mixture
ns	Number of specie

Introduction

Although there are a vast number of applications for a single-component ideal gas computer program, the restriction to a single component excludes simulation of many important multispecies flows in the aerospace industry. The removal of this restriction requires the inclusion of multicomponent, chemically reacting models in the simulation. Inclusion of a multispecies capability in a computational fluid dynamics program is an entrance into multidisciplinary modeling that results in a plethora of physical and numerical models that may or may not be included in the simulation. Because of the complexity and number of models that could be included in a multispecie program, it is desirable to begin with a well planned computational framework in which models can be modified, added, or deleted with relative ease. Therefore, these programs are generally not static and are continuously being upgraded to include improvements and to satisfy new requirements.

The Wind program[1] is designed to allow a variety of equation and variable sets. The modular structure and the memory allocation method make it relatively easy to add or modify submodels. The multicomponent thermal, transport, and reaction computations are located primarily in a directory (chem) that is separated from the Navier-Stokes equation solution directory (struct).

Several modifications to the multispecie chemistry models have been incorporated since Wind became an NPARC Alliance flow solver. These modifications include: updated thermodynamic data; beta/gamma corrections; computation of the equilibrium constant from thermodynamic data; debugged Wilke diffusion; addition of an effective binary diffusion model; variable third-body efficiencies; Pade solution of the ordinary differential equations governing species equations, with chemical kinetics; and a preprocessor chemistry input manager.

Thermodynamic Models

The curve fit format for thermodynamic data was updated to allow the option of using either the original Wind format or the current format used and supported by NASA Glenn. This new format as prescribed in NASA TP3287,[2] and a slightly modified version in the CEA program user's manual[3] is defined as follows:

$$C_p^0 = a_1 T^{-2} + a_2 T^{-1} + a_3 + a_4 T + a_5 T^2 + a_6 T^2 + a_7 T^4 + a_8 T^5 \tag{1}$$

$$\frac{H^0(T)}{RT} = -a_1 T^{-2} + a_2 T^{-1} \ln T + a_3 + a_4 \frac{T}{2} + a_5 \frac{T^2}{3} + a_6 \frac{T^3}{4} + a_7 \frac{T^4}{5} + a_8 \frac{T^5}{6} + \frac{b_1}{T} \tag{2}$$

$$\frac{S^0(T)}{RT} = b_2 - a_1 \frac{T^{-2}}{2} - a_2 T^{-1} + a_3 \ln T + a_4 T + a_5 \frac{T^2}{2} + a_6 \frac{T^3}{3} + a_7 \frac{T^4}{4} + a_8 \frac{T^5}{5} \tag{3}$$

These coefficients are contained in the thermo files that are supplied for input with several current NASA chemistry programs. The format for specifying the thermodynamic data and the definition of input data are defined in the CEA manual. This format is invoked in the Wind Chemistry (.chm) files by inserting a line, starting in column one, containing “NASA3287” after the line specifying the number of species and before the beginning of the thermodynamic data. The new input is much more flexible than the existing format in that the temperature ranges and number of coefficient sets can vary with specie. To be consistent with the complete input data set, the units in the above curves are Joules, moles, and deg Kelvin.

The original Wind format that defines specific heat as shown below is still supported:

$$\frac{C_p^0}{R} = a_1 + a_2 T + a_3 T^3 + a_4 T^4 + a_5 T^4 \qquad (4)$$

For this format, the "a" coefficient definitions given by Gordon[4] must now be used to compute enthalpy as:

$$\frac{H^0(T)}{RT} = a_1 \ln T + a_2 T + \frac{a_3}{2} T^2 + \frac{a_4}{3} T + \frac{a_5}{4} T^4 + a_7 \qquad (5)$$

and entropy (needed for the equilibrium constant) as:

$$\frac{S^0(T)}{R} = a_1 \ln T + a_2 T + \frac{a_3}{2} T^2 + a_4 \frac{T^3}{3} + a_5 \frac{T^4}{4} + a_7 \qquad (6)$$

The heat of formation is computed internally from these curves as the species enthalpy at 298.15 K of temperature.

In the new version of the Wind code we have distinguished between γ and β. The former is used for the calculation of sound speed and the later for calculation of enthalpy or pressure from the conserved energy. Gamma is calculated from the thermodynamic data in all Wind versions as:

$$\gamma = \frac{C_p(T)}{C_p(T) - RT} \qquad (7)$$

Beta, which originally was defined as:

$$\hat{\beta} = \frac{\int C_p(T)dt / \int dT}{(\int C_p(T)dt / \int dT) - R} \qquad (8)$$

has been redefined as:

$$\beta = \frac{H^0}{H^0 - RT} = \frac{H^0}{E^0} \qquad (9)$$

It is not uncommon for temperature to be less than the minimum range of the thermodynamic curve fits in high Mach number flow. Currently, exceeding the lower or upper temperature range causes the program to stop with an error message. The thermal properties can be extrapolated beyond the limits by invoking test option 71. A process to automatically extend the thermodynamic data beyond the low-temperature range may be considered for future versions. However, currently the best method to handle low-temperature flow is to compute an additional temperature range to the thermodynamic data. Generally, for monatomic molecules the lowest temperature range can be recopied with the temperature limits replaced by the lower range to obtain the additional range. Usually for diatomic molecules C_p is nearly constant or slowly varying so that its curve fit can be reduced to either an a_1 coefficient (constant C_p) or a_1 and a_2 coefficients (linear C_p) with respect to Eqs. (4-6). The value of C_p at the lowest temperature can be obtained from the JANAF tables or can be estimated using the number of molecular degrees of freedom, ξ, from statistical mechanics as shown below:[5]

$$C_p = \frac{\xi + 2}{2} R \qquad (10)$$

The a_6 and a_7 coefficients must be set to match the enthalpy and entropy, respectively, at the minimum temperature of the adjacent temperature range.

Reaction Models

Two general types of chemical reactions are allowed: dissociation and exchange.

Dissociation reactions in Wind are of the form:

$$\nu'_1 [S_1] + M_s \Leftrightarrow \nu''_1 [S_2] + \nu''_2 [S_3] + M_s \qquad (11)$$

or

$$\nu'_1 [S_1] + \nu'_2 [S_2] + M_s \Leftrightarrow \nu''_1 [S_3] + M_s \qquad (12)$$

While exchange reactions are of the form:

$$\nu'_1 [S_1] + \nu'_2 [S_2] \Leftrightarrow \nu''_1 [S_3] + \nu''_2 [S_4] \quad (13)$$

The law of mass action gives the molar production rate of a molecular species due to all reactions included in a chemistry model as

$$\dot{\omega}_s = M_s \sum_{r=1}^{nr} (\nu''_{s,r} - \nu'_{s,r}) \left(k_{f,r} \prod_{s=1}^{ns} [\chi_s]^{\nu'_{s,r}} - k_{b,r} \prod_{s=1}^{ns} [\chi_s]^{\nu''_{s,r}} \right) \quad (14)$$

Wind contains three methods of computing the reaction rate coefficients, $R_{f,r}$ and $k_{b,r}$, for finite rate chemistry. All of the reaction options in Wind compute the forward kinetic rate coefficient using the modified Arrhenius form

$$k_{f,r} = C_f T^{S_f} e^{-D_f/(\kappa T)} \quad (15)$$

The first method computes the backward rate as the quotient of the forward rate coefficient and the equilibrium constant which is obtained from a fourth-order, temperature-dependent polynomial:

$$k_{b,r} = k_{f,r} / K \quad (16)$$

where

$$K = \exp(a_1 + a_2 Z + a_3 Z^2 + a_4 Z^3 + a_5 Z^4) \quad (17)$$

and

$$Z = (10000)/T \quad (18)$$

Since the equilibrium constant here does not appear to be a function of pressure, if the number of moles of reactant does not equal the number of moles of product in a given reaction, there will be some error in the equilibrium constant. If the reaction occurs at the reference pressure, generally one atmosphere, then no correction is required.

The second method also computes the backward rate coefficients but uses the modified Arrhenius equation

$$k_{b,r} = C_b T^{S_b} e^{-D_b/(\kappa T)} \quad (19)$$

A third method, used only for one- or two-equation global reactions, calculates only the forward rate coefficient.

Quite often parameters for computing reaction rate coefficients are reported for only one direction and coefficients for computing the equilibrium constant from a polynomial are difficult to find. However, the thermodynamic data contain enough information to compute the equilibrium constant and thus the reverse rate coefficient without further input. The relationship between Gibbs function and the equilibrium constant is documented in textbooks. The Gibbs function for a reaction at standard pressure is obtained from the thermodynamic data as:[5,6]

$$\Delta G_R(T, p^0) = \sum \upsilon_p g_p - \sum \upsilon_r g_r \quad (20)$$

where

$$g(T, p^0) = \left(\frac{H^0}{RT} - \frac{S^0}{R} \right) RT \quad (21)$$

Here υ_p and υ_r are the stoichiometric coefficients of the reaction products and reactants respectively. The molar concentration equilibrium constant is then given by Ref. 5:

$$K_c = \exp\left(\frac{-\Delta G_R(T, p^0)}{RT} \right) \left(\frac{RT}{P^0} \right)^{\Sigma \upsilon_r - \Sigma \upsilon_p} = \exp\left(\frac{-\Delta G_R(T, p^0)}{RT} \right) \left(\frac{0.012186}{T} \right)^{\Sigma \upsilon_p - \Sigma \upsilon_r} \quad (22)$$

when R = 82.05 cm^3 atm g-$mole^{-1}K^{-1}$ and p^0 is equal to one atmosphere of pressure.

The computation of the above thermodynamic properties had been included as code fragments in subroutines where they were needed. In the current versions of Wind, the thermodynamic properties C_p, H, S, and g (the specific heat, enthalpy, entropy, and Gibbs function, respectively) are computed in function routines. The NASA curve fits by Gordon, et. al.[4] or McBride, et. al.[2] should be used for this reaction option. If the older, five-coefficient C_p model is used, it should be put into the Wind format. The computation of C_p, H, and log K_p from the NASA 3287 curve fits for H_2O have been com-

pared with tabulated JANAF[7] results, and excellent agreement is achieved as shown in Fig. 1. Computed NASA SP-273 curves were nearly identical to the result shown with the exception that this lower-order fit extrapolated C_p better at low temperature than did the newer fits.

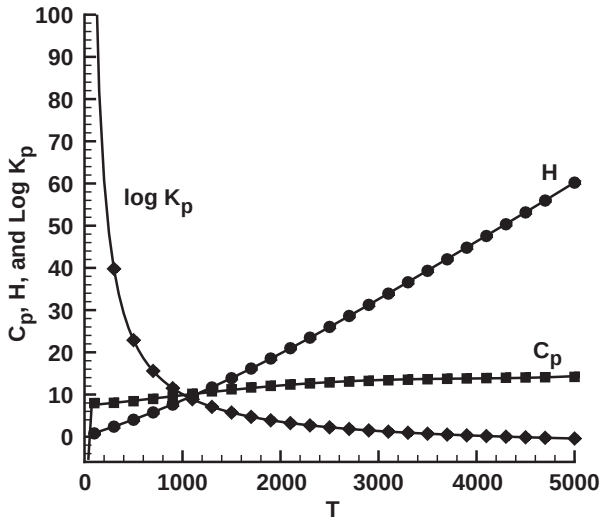

Fig. 1. Comparison of H_2O Curve Fit Thermo Properties with JANAF Table

For dissociation, the reaction rate depends on both gas temperature and the collision partner, M_s. To account for this dependence, when the Arrhenius collision parameters, C_f and C_b, are multiplied by molar concentration, three forms may be used:

$$[C_r] = \sum_{s=1}^{ns} [\chi_s] C_{r,s}, \tag{23}$$

$$[C_r] = \hat{C}_r \sum_{s=1}^{ns} [\chi_s] E_{r,s}, \tag{24}$$

or

$$[C_r] = \hat{C}_r \sum_{s=1}^{ns} [\chi_s]. \tag{25}$$

Here $[C_r]$ represents the product of the molar concentration of the third bodies with the forward or backward reaction rate coefficient. These coefficients are seen to increase the order of dependence on molar concentration when they are substituted into the species production equations, above. Only the first rate method, which computes the equilibrium constant from a fourth-order polynomial and applies Eq. (23), includes variable third-body efficiencies for kinetic rates in the currently released versions of Wind. Alternately, this method can also use the third form above, Eq. (25), with an average collision coefficient. The other methods allow only an average collision coefficient. However, reaction rate data sets often use the second form, Eq. (24), above, to include the effect of individual third body efficiencies, where a nominal collision coefficient is specified and efficiency multipliers, $E_{r,s}$, are specified to account for variations among the specie. This method of accounting for specie-dependent, third-body efficiencies has been programmed into the last two reaction rate methods in a developmental version of Wind, and a test case has been computed to examine the effect of third-body efficiency model differences.

Transport Models

There are four transport models in Wind: 1) Constant viscosity, 2) Sutherland's formula, 3) Keye's-Sutherland's formula, and 4) Wilke's mixing rule. The first three models apply to a single-component gas. Viscosity is computed or set by these models with the thermal conductivity, k, and diffusivity, D, being computed from the Prandtl and Lewis numbers, respectively, as

$$k = \mu C_p / P_r \tag{26}$$

$$D = k L_e / \rho C_p \tag{27}$$

The last three models all use Sutherland's law to calculate viscosity as follows:

$$\frac{\mu}{\mu_0} = \left(\frac{T}{T_{0\mu}}\right)^{\frac{3}{2}} \left(\frac{T_{0\mu} + S_\mu}{T + S_\mu}\right) \tag{28}$$

In the Keye's-Sutherland's method, the above formula is blended with Keye's formula to give viscosity below temperatures of 180^oR as:

$$\frac{\mu}{\mu_{0K}} = \left(\frac{T}{T_{0\mu K}}\right)^{\frac{1}{2}} \left(\frac{T_{0\mu K} + S_{\mu K}}{T + S_{\mu K}}\right) \tag{29}$$

The Wilke's mixing rule method also computes the thermal conductivity using Sutherland's rule:

$$\frac{k}{k_0} = \left(\frac{T}{T_{0k}}\right)^{\frac{3}{2}} \left(\frac{T_{0k} + S_k}{T + S_k}\right) \tag{30}$$

Wilke's mixing rule,[8] which is the only option that accounts for the actual composition of the gas, caused an error in early versions of the code but is fully operational now and is recommended for gas mixtures and single-component gases that are not similar to air. Wilke's method is applied by first computing the viscosity, μ_i, and thermal conductivity, k_i, of each molecular species using Sutherland's equations (above); then the mixture properties are obtained as

$$\mu_{mix} = \sum_{i=1}^{ns} \left(\frac{\chi_i \mu_i}{\sum_{j=1}^{ns} \chi_j \phi_{if}} \right) \tag{31}$$

and

$$k_{mix} = \sum_{i=1}^{ns} \left(\frac{\chi_i k_i}{\sum_{j=1}^{ns} \chi_j \phi_{if}} \right) \tag{32}$$

where the intercollision parameter ϕ_{ij} is given by

$$\phi_{ij} = \frac{[1 + (\mu_1/\mu_j)^{1/2} (M_i M_j)^{1/4}]^2}{[8(1 + M_i/M_j)]^{1/2}} \tag{33}$$

The mixture diffusion coefficient is determined from the thermal conductivity, Eq. (32), and the Lewis number, which is assumed to be equal to 1, as

$$\begin{aligned} D_{mix} &= k_{mix} L_e / (\rho_{mix} C_{p_{mix}}) \\ &= k_{mix} / (\rho_{mix} C_{p_{mix}}) \end{aligned} \tag{34}$$

In a real mixture of gases, each molecular species diffuses at a rate determined by the concentration of each species and its binary diffusion rate with respect to every other specie. Approximating the molecular diffusion with a single mixture diffusivity can cause inaccuracies when large variations in molecular weight and/or large variations in bimolecular collision integrals exist. The complete solution of multicomponent diffusion requires computing the binary diffusivity of every molecular pair and the binary diffusion of every molecular pair. Because full multicomponent diffusion is computationally expensive, an effective binary diffusion model approximation is often used. In the effective binary diffusion model, the "effective binary" diffusivity of each species with respect to the mixture is computed thus:[9]

$$D_{i,\,mix} = (1 - \chi_i) \left(\sum_{j \neq i}^{ns} \chi_j / D_{ij} \right)^{-1} \tag{35}$$

The diffusivity of each species within the mixture can be computed by the Chapman-Enskog formula[8] for an ideal gas as:

$$D_{ij} = 0.0018583 \frac{\sqrt{T^3 \left(\frac{1}{M_i} + \frac{1}{M_j} \right)}}{p \sigma_{ij}^2 \Omega_{D,\,ij}} \tag{36}$$

The units for D_{ij} are cm^2/sec with p in atm and T in K. The effective collision diameter, σ_{if}, in Angstroms, is computed as

$$\sigma_{ij} = \frac{1}{2} (\sigma_i + \sigma_j) \tag{37}$$

If the intermolecular potential of the molecular pair is represented by Lennard-Jones function:

$$\phi_{ij}(r) = 4 \varepsilon_{ij} \left[\left(\frac{\sigma_{ij}}{r} \right)^{12} - \left(\frac{\sigma_{ij}}{r} \right)^{6} \right] \tag{38}$$

where ε_{ij} is the maximum attractive energy between molecules i and j, and r is the distance between the molecules, then the nondimensional collision integral, $\Omega_{D,ij}$ can be computed as a function of kT/ε_{ij} only where ε_{ij} is computed as: $\varepsilon_{ij} = \sqrt{\varepsilon_i + \varepsilon_j}$. In turn, $\Omega_{D,ij}$ can be calculated by the Neufield relation:

$$\begin{aligned} \Omega_{D,\,ij} = &\frac{A}{(T^*)^B} + \frac{C}{\exp(DT^*)} \\ &+ \frac{E}{\exp(FT^*)} + \frac{G}{\exp(HT^*)} \end{aligned} \tag{39}$$

where $T^* = kT/\varepsilon_{if}$, A = 1.06036, B = 0.15610, C = 0.19300, D = 0.47635, E = 1.03587, F = 1.52996, G = 1.76474, and H = 3.89411.

Thus, to compute the binary diffusion coefficients, the only additional input to Wind is the Lennard-Jones parameters, σ_i and ε_i, for each molecule; these are tabulated in a number of references

(for example Bird, Stewart, and Lighfoot[9]). Effective binary diffusion enters into the species conservation equation through the term:

$$\nabla \cdot \rho D_{i,\,mix} \nabla \rho_i / \rho \,. \qquad (40)$$

where ρ_i/ρ is the mass fraction of the i^{th} species.

Operator Splitting Method

The original implementation of the chemistry model in the Wind code is explained in Ref. 10 and is a direct inclusion of the production term from the species continuity equations as source terms for the chemistry equation set. The addition of these source terms for certain chemical reactions can make the system of equations stiff. This stiffness usually arises from the disparate time scales between the chemical reaction time and the fluid dynamic time scale. In the stiff system of equations the chemical time step is usually several orders of magnitude smaller than the fluid dynamic time scale. One approach that was successfully used in Ref. 11 is to separately integrate the reaction source terms with an Ordinary Differential Equation (ODE) solver. In this approach the chemistry source term in each cell is treated as an ordinary differential equation and is integrated over the fluid time scale.

The rational Pade approximation has been employed to integrate the chemistry production term over a fluid time step. In this approach, subiterations may be performed to improve the equation set stability. The description of this approach can be found in Ref. 11.

If the vector of the species concentrations at a particular location is represented by $\vec{C}(t)$ and the production terms are given by $\dot{\vec{C}}(\vec{C}, T)$, with T being the local temperature, then the fifth-order Pade approximation is

$$\vec{C}(t+\Delta t) = \vec{C}(t) + \Delta t\left(I - \frac{\Delta t}{2}J + \frac{\Delta t^2}{12}J^2\right)^{-1}\dot{\vec{C}}, \quad (41)$$

Where I is the identity matrix and J is the Jacobian $\partial\dot{\vec{C}}/(\partial\vec{C})$. The Jacobian is computed analytically during the generation of the reaction rates. Note that this evolution relation is at constant temperature whereas the actual physics occurs at constant enthalpy. In the future an additional solution loop can be added to the present scheme to ensure that enthalpy is conserved; however, this is not believed to be necessary for current applications.

Previous investigators have applied various filters to the species concentration and source terms. We have not implemented any filter because of the Wind framework, which sweeps through the I-planes in a zone to determine the chemical source terms. This capability can be invoked through test option 92. The value of this test option represents the number of subiterations of the Pade approximation to be performed for each fluid time-step.

In order to investigate the impact of the operator splitting on a stiff system of chemically reacting equations, we have chosen to resolve the premixed H_2-air flow through an axisymmetric nozzle. The inflow conditions are Mach = 1.4, T = 1900K, p = 0.081 Mpa, and fuel/air ratio= 0.3. The nozzle radius is represented by $r(x) = 0.5 + 0.5 \sin(\pi x/4)$, for $0 \le x \le 2$; x is in meters. An axisymmetric grid of 5×101 was used to approximate the quasi-1D theory. The results at the nozzle centerline are compared with the results obtained by Drummond.[12] The operator-splitting scheme showed significant improvements with the Wind point implicit scheme. The full implicit scheme showed no advantage over the point implicit scheme and requires more CPU time than the former. The normalized CPU times required to reach steady state at different CFL numbers with different numbers of operator splitting subiterations are shown in Table 1. The normalized time is based on the time required (1300 sec) by the baseline scheme to reach steady state without any operator splitting.

Table 1. CPU Time Per Node-Iteration (microsec)/ Normalized Time To Convergence for Various Solutions To the Axisymmetric Nozzle Case Using the Point Implicit Time Integration Operator

Subiterations	CFL = 0.10	CFL = 0.15	CFL = 0.20
1	Solution Diverged		
2	228/0.336	Solution Diverged	
3	332/0.510	Solution Diverged	
4	445/0.885	508/0.391	452/0.337

* This simulation was performed using double precision for the chemistry source terms.

Figure 2 shows the convergence of the governing equation with and without the operator splitting. The operator splitting has no impact on the convergence or on the stability of the governing equations in the explicit mode. However, it has a substantial impact on the convergence and stability of the governing equations in the implicit mode. Figure 3 compares the results with and without the operator-splitting scheme vs. the results from Ref. 12. The Wind results without the operator-splitting scheme agree well with the quasi one-dimensional results of Ref. 12. The results with the operator-splitting scheme show a delay in the reaction time.

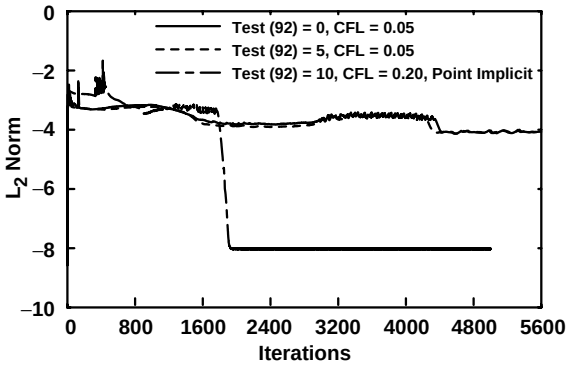

Fig. 2. Convergence History for Axisymmetric Nozzle with Different Subiterations

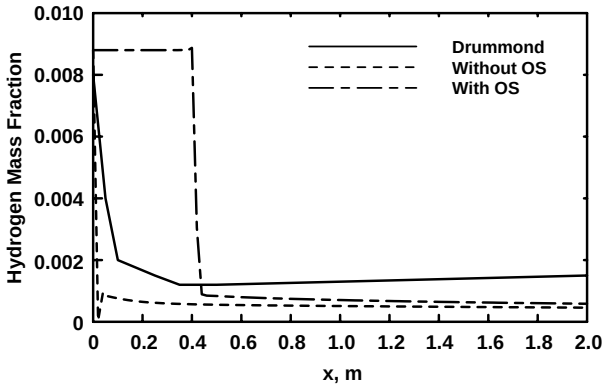

Fig. 3. Comparison of H_2 Dissociations with Different Schemes

This delay in reaction happens with the operator-splitting whenever there is no geometric flame holder to fix the ignition point; it needs to be considered when this type of computation is performed.

The CHMGR (Chemistry Manager) Utility

As can be seen from the preceding paragraphs, three types of data are needed to execute a chemically reacting computation: 1) thermodynamic data, 2) finite rate coefficients, and 3) transport properties. The CHMGR, a utility program supplied with Wind, has been written to facilitate the assembly of this data and to create the required .chm file. This program can either create a .chm file from scratch using included databases or modify an existing .chm file. The program can be run in a menu-driven text mode or through a user-friendly Graphical User Interface (GUI). The GUI generates the text menu commands and user input needed by the CHMGR executable. The menu driver allows easy access to various user-supplied or Wind library data sources.

To construct the thermodynamic data for the .chm file from scratch, the user selects the thermo data input option. Wind or NASA GRC can be selected as the thermodynamic data file format to be read. The data can be written out in Wind or NASA GRC format. The NASA TP 3287 format is not currently read or written by the chemistry manager. A C_p curve fit manager can also create the thermo data. Tabulated values of C_p/R versus temperature are input from a source such as the JANAF tables to use this option. The data are fit to a fourth-order polynomial in temperature. If data are to be read, the directory containing the input file is selected, and then the input file is selected. The chemistry manager lists the specie names contained in the file. Species can be added to or deleted from the list. The specie data can come from multiple databases if desired.

The transport property and the kinetic reaction data are created similarly. The transport data can be read in Wind or NASA GRC format. Construction of the reaction data for the .chm file is not fully operational.

An option exists to select a Wind chemistry file as a baseline model. The procedures outlined above for creating chemistry files can also be used to modify a baseline file. Detailed instructions for using the CHMGR utility are given in the Wind Utilities section of the online documentation.

Demonstration Cases

Two demonstration cases were computed to examine the influence of third-body reactions and effective binary diffusion on the flow-field solution.

Mach 4.0 Shock-Initiated Combustion

The first case is a 10-deg wedge with a freestream Mach number of 4.0 at 1 atm of pressure. The gas is premixed H_2/air at a stoichiometric ratio of one and at a temperature of 900 K, which is below the ignition temperature of the mixture. This case, previously computed by Shuen[13] and Chisomboon,[14] indicates the effect of chemistry model on temperature, pressure and molecular concentrations. The chemistry model used by Shuen was a 14-step reaction set obtained by Hitch[15] by reducing a more complete set compiled by Westbrook.[16] No experimental data were given for this case. Wind computations employed three different reaction sets for this example: 1) the 17-reaction Westbrook model, 2) the 14-reaction Hitch model with variable third-body efficiency,[17] and 3) the 14-reaction Hitch model with unity third-body efficiency. Note, that the 1986 Hitch model used by Shuen was derived from a Westbrook set, while the 1988 Hitch model was derived mostly from a Tsang reaction set.[18] The 1986 Hitch model was not obtained, but it is assumed that it is not the same as the 1988 Hitch model. The Westbrook and Hitch reaction sets input to Wind are shown in Tables 2 and 3,

Table 2. Westbrook Hydrogen-Air Reaction Model

Reaction	S_f S_b	D_f/κ D_b/κ	C_f C_b
O_2 = O + O	0 –0.28	5.7870E+04 0	5.12E+15 4.67E+15
H_2 = H + H	0 0	4.8309E+04 0	2.19E+14 3.02E+15
H_2O = OH + H	0 –2.0	5.2838E+04 0	2.19E+16 1.41E+23
OH = O + H	–1.0 0	5.2194E+04 0	7.94E+19 1.00E+16
H_2O_2 = OH + OH	0 0	2.2896E+04 –2.551E+03	1.20E+17 9.12E+14
HO_2 = H + O_2	0 0	2.3097E+04 –5.030E+02	2.29E+15 1.66E+15
O_2 + H = OH + O	0 0	8.4430E+03 3.4219E+03	1.86E+14 1.47E+13
H_2 + O = OH + H	1.0 1.0	4.4786E+03 3.4973E+03	1.82E+10 8.32E+09
H_2O + O = OH + OH	0 0	9.2341E+03 5.5300E+02	3.38E+113 3.16E+12
H_2O + H = OH + H_2	0 0	1.0215E+04 2.5916E+03	9.54E+13 2.19E+13
H_2O_2 + OH = H_2O + HO_2	0 0	9.0579E+02 1.6500E+04	1.00E+13 2.82E+13
HO_2 + O = OH + O_2	0 0	5.0322E+02 2.8487E+04	5.01E+13 6.45E+13
HO_2 + H = OH + OH	0 0	9.5611E+02 2.0179E+04	2.51E+14 1.20E+13
HO_2 + H = H_2 + O_2	0 0	3.5225E+02 2.9086E+04	2.51E+13 5.49E+13
HO_2 + OH = H_2O + O_2	0 0	5.0322E+02 3.7167E+04	5.01E+13 6.31E+14
H_2O_2 + O_2 = HO_2 + HO_2	0 0	2.1457E+04 5.0322E+02	3.98E+13 1.00E+13
H_2O_2 + H = HO_2 + H_2	0 0	1.8871E+03 9.41022+03	1.69E+12 7.24E+11

Table 3. Hitch Hydrogen-Air Reaction Model with Third Body Efficiency

Reaction	S_f	D_f/κ	C_f
H + H = H_2	–1.30	0	5.44E+18
Third Body Efficiency 2			
H_2O 18.3			
H_2 2.5			
H + OH = H_2O	–2.0	0	2.21E+22
Third Body Efficiency 2			
H_2O 6.3			
H_2 2.5			
H + O_2 = HO_2	–1.62	0	2.08E+20
Third Body Efficiency 2			
H_2O 16.25			
H_2 2.6			
HO_2 = O + OH	–0.43	3.2206E+04	6.80E+19
Third Body Efficiency 0			
H_2O_2 = OH + OH	–4.86	2.6776E+04	1.29E+33
Third Body Efficiency 2			
H_2O 6.0			
H_2 2.5			
H_2 + OH = H_2O + H	2.0	1.4890E+03	6.38E+06
O_2 + H = OH + O	–0.9	8.7459E+03	1.69E+17
H_2 + O = OH + H	2.80	2.9780E+03	1.08E+04
HO_2 + H = H_2 + O_2	0	1.0693E+03	6.62E+13
HO_2 + H = OH + OH	0	4.3971E+02	1.69E+14
HO_2 + O = OH + O_2	0	–1.998E+02	1.75E+13
HO_2 + OH = H_2O + O_2	–1.0	0	1.45E+16
H_2O_2 + H = HO_2 + H_2	0	3.9715E+03	4.82E+13
HO_2 + HO_2 = H_2O_2 + O_2	0	0	1.81E+12

respectively. These tables are in Wind format with the exception of the representation of the stoichiometric equations. Only the nonunity values of third-body efficiency are shown in the Hitch table as indicated.

A plot of the pressure contours computed by Wind is shown in Fig. 4 to define the case geometry and indicate the shock location. The overall dimensions of the solution domain are 3 × 2 cm. The wedge starts at 1 cm and is 2 cm long. The dark, thick group of contour lines indicates the location of the shock wave that initiates combustion by increasing temperature.

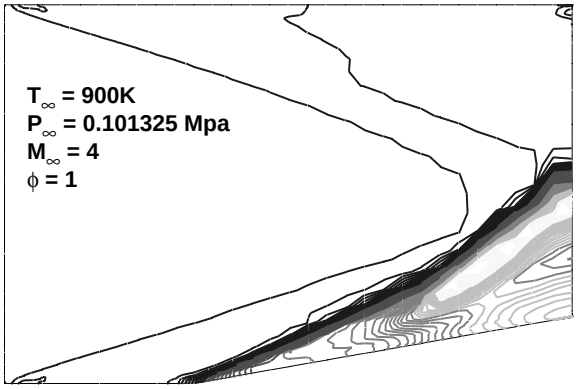

Fig. 4. Wind Static Pressure Contours on Mach Wedge

Figure 5 shows the effect of variable third-body efficiency on the extent of the combustion region. In this plot, the results for third-body efficiency = 1 have been flipped 180 deg for comparison with the variable third-body model.

The combustion regions lie under the dark group of H_2O contours. It can be seen that the higher third-body efficiencies of H_2O and H_2, and thus increased dissociation reaction rates, create a thicker combustion zone. The computation was also run with variable third body efficiency and the Wilke diffusion model instead of the effective binary diffusion model. Since there was very little difference in contours for the two diffusion models, the Wilke contours are not plotted.

In Figs. 6 through 9, the results of the Wind models are compared with each other and with the results presented in the paper by Shuen. Figure 6 shows the predicted pressures along a line 0.13 cm above the lower wall. The Wind results with variable third-body efficiency and effective binary diffusion are indicated by the curve labeled Hitch 3BD. The Wind results without these models are labeled Hitch. It can be seen that the Hitch curve is closer to the Shuen curve, while the Hitch 3BD curve is closer to the Chitsomboon curve. The beginning of the pressure rise is similar for all the curves, and the rise in pressure is similar for all but the Chitsomboon curve. The final pressure of the Hitch curve is highest, while the Chitsomboon and three-body curve result in almost the same peak. It is unexpected that the faster, third-body rates would lower the final pressure. However, these results are only along a single line, and the peaks for the whole flow field were close.

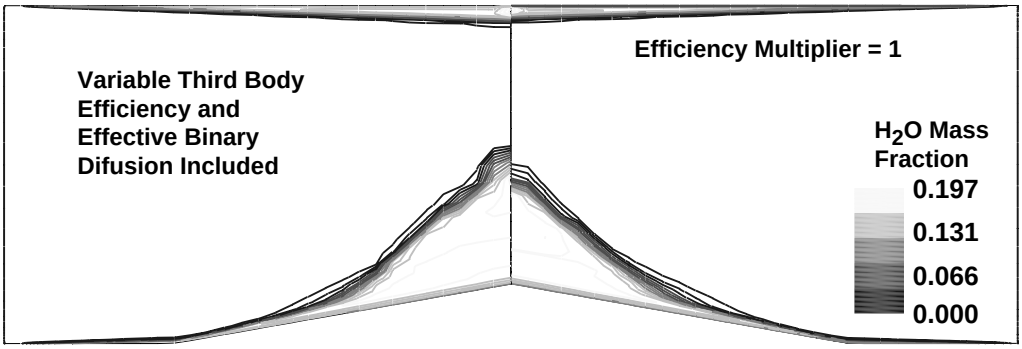

Fig. 5. Effect of Variable Third Body Efficiency on Combustion Region

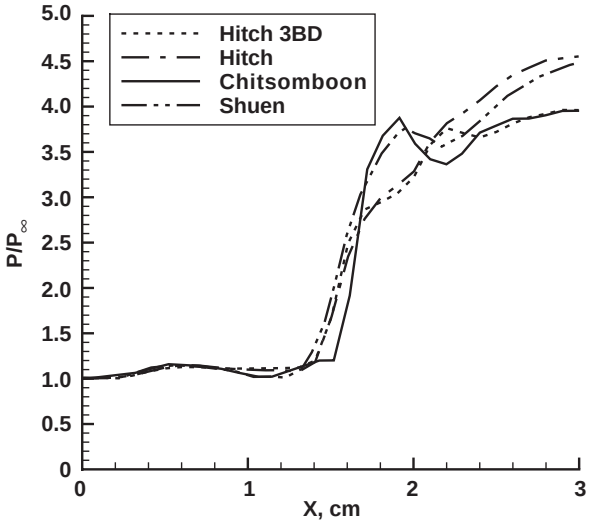

Fig. 6. Comparison of Pressure 0.13 cm off Lower Wall

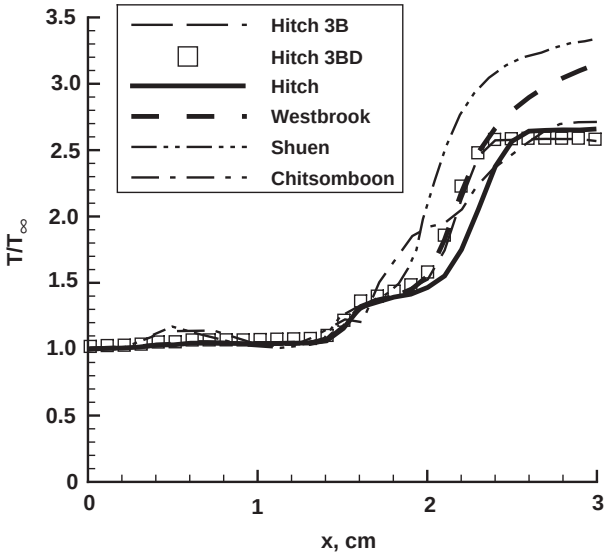

Fig. 7. Comparison of Temperature 0.13 cm off Lower Wall

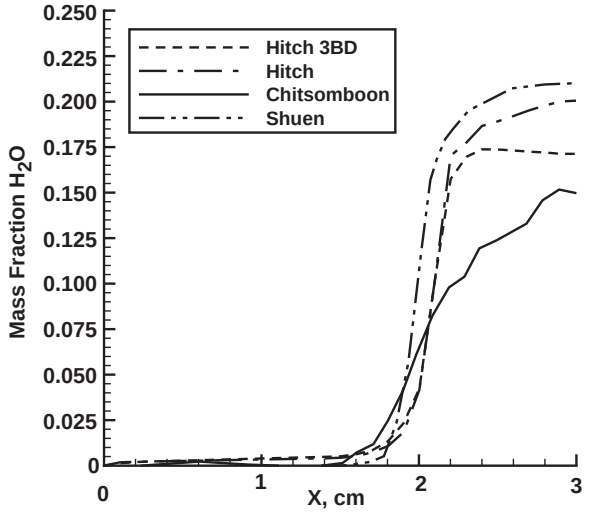

Fig. 8. Comparison of H_2O Concentration 0.13 cm off Lower Wall

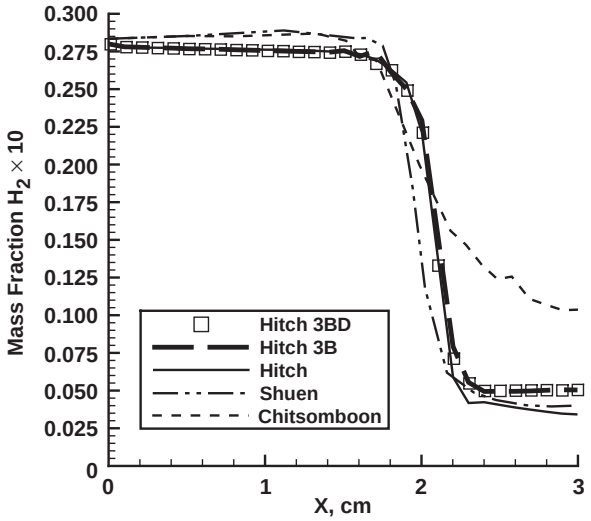

Fig. 9. Comparison of H_2 Concentration 0.13 cm off Lower Wall

Figure 7 shows the nondimensionalized temperature results along the same 0.13-cm line. The first four curves in the legend are Wind results for four different chemistry/diffusion models. The first two curves include variable third-body efficiency with and without effective binary diffusion. Effective binary diffusion shifts the temperature curve very slightly upstream. There are some oscillations near the inflow boundary in the Shuen and Chitsomboon curves, but the onset of combustion is essentially the same for all curves at approximately 1.4 cm from the inlet boundary. The Wind results ramp up later than the two other computations in the 2-cm region. The Wind Hitch results level off at about the same final value as the twp reaction global model used by Chitsomboon, while the Westbrook reaction model temperature continues to climb similar to the results of Shuen. The Hitch models with variable third-body efficiency are seen to significantly shift the temperature curve upstream compared to the Hitch model with constant efficiency. However, a slightly lower temperature peak results. All the Wind Hitch models result in a flat constant temperature section near the outflow boundary. These curves appear to have hit a limit. It is suspected that this is the result of using the equilibrium constant predicted from the thermodynamic data to obtain the backward rate coefficient, since the Wind Hitch model used the thermodynamic equilibrium constant, while the Wind Westbrook model used both forward and backward Arrenhius rates.

The amounts of H_2O predicted along the 0.13-cm line are shown in Fig. 8. The Shuen computation results in the highest concentration of H_2O, while the Chitsomboon curve is substantially lower than the rest. Since models with and without effective binary diffusion were very close, only one variable third-body curve is shown. The model with variable third body efficiency is seen to peak lower than the model with constant efficiency. The shapes of all the curves except the two-reaction global model are similar. Ignition is delayed in the Shuen results compared to the Wind results; however, the major ramp-up of H2O is approximately half a centimeter further upstream for the Shuen curve.

The consumption of H_2 along the 0.13-cm line is indicated in Fig. 9. The results are consistent with the H_2O production curves. It can be seen that the global reaction model used by Chitsomboon again deviates substantially from the other computations. The other models agree reasonably well with the same trends as the H_2O curves. The variable third-body efficiency is seen to result in less H_2 consumption along this line.

Subsonic Diffusion

A low Mach number mixing layer case was computed to examine the influence of diffusion model on molecular concentration. The demonstration case is for axisymmetric mixing of air with hydrogen. For this case, hydrogen is injected at

Mach 0.043 through a 0.381-cm radius tube at the center of a 15.25-cm radius pipe in which air is flowing at Mach 0.043. As indicated above, Wilke's formula computes an averaged diffusion coefficient that is applied to each species, while the effective binary diffusion model computes an individual diffusion coefficient for each species with the mixture. The previous high Mach number premixed case showed little sensitivity to the diffusion models considered. However, in Fig. 10, where the zero H_2 contour line indicates the mixing layer thickness, a substantial difference is seen between the two models. Not only is the mixing layer much thicker for binary diffusion, but the layer is also more stable, as indicated by the wavy contours near the axis of symmetry for the Wilke case. Figure 11 shows a cross-stream plot of the H_2 concentration at the outflow boundary. It is seen that the binary centerline value is 20 percent lower than the Wilke value and that the effective binary curve extends beyond the Wilke curve.

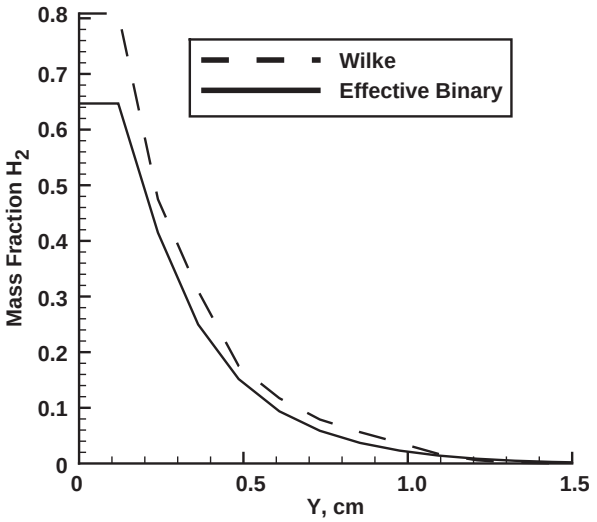

Fig. 11. Concentration of H_2 at the Outflow Boundary

Future Upgrades

While Wind has a very general chemistry capability, there remain some improvements that might be desirable. The option to include third-body efficiency should be included in the next Wind release. Also, a default method of computing thermodynamic properties beyond the low-temperature range may be included. Inclusion of turbulence chemistry interactions may be desirable, especially for low Mach number application.

A large difference in molecular weights on highly stretched grids has been known to reduce stability in some cases. It may be desirable to investigate methods of increasing robustness for these cases. Full, implicit solution of the bulk flow conservation equations together with the specie conservation equations and additional or improved smoothing might also increase robustness.

The multicomponent thermodynamic properties should be fully implemented for post processing. Accurate computation of multispecies total conditions requires computation of entropy to evaluate isentropic processes. Computation of entropy using the curves above should be included in post processors.

A multiphase module is currently being added to increase the range of application. The model being added employs Lagrangian particle tracking and will include drop evaporation and spray injection.

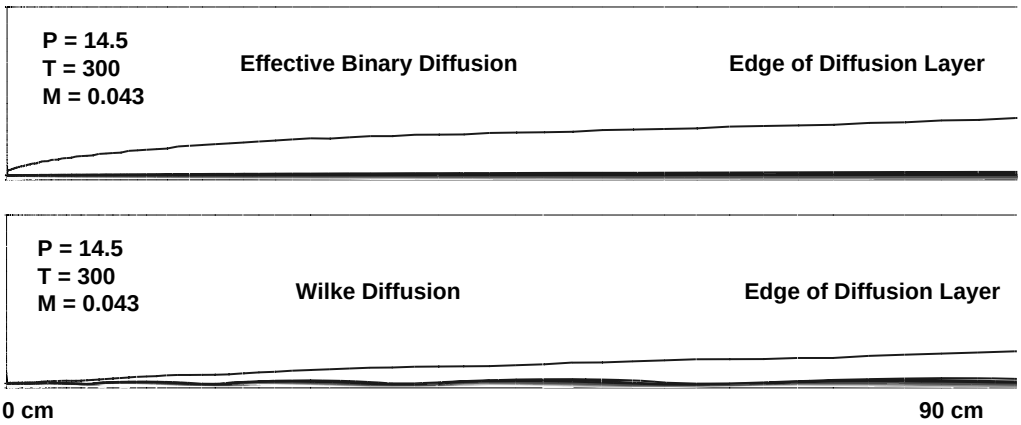

Fig. 10. Comparison of H_2 Diffusion Layer Thickness for Mach 0.043 Flow

Summary

A number of updates have been incorporated in Wind to improve the efficiency, accuracy, and robustness of the flow solver. Thermodynamic properties can be included using current NASA GRC formats. Third-body efficiency and binary diffusion models have been developed, and the influence of these models has been examined. The Pade method, which accounts for disparate time scales in systems of ordinary differential equations, has been incorporated in order to solve the species conservation equations in an efficient and robust manner. The Wind program continues to be upgraded as more efficient and/or accurate methods become available.

References

1. Nelson, C. C., and Power, G. D., "CHSSI Project CFD-7:The NPARC ALLIANCE Flow Simulation System," AIAA-2001-0594, January 8-11, 2001.

2. McBride, B.J., Gordon, S. and Reno Sanford, A., "Thermodynamic Data for Fifty Reference Elements," NASA TP-3287, 1993.

3. McBride, B. J., and Gordon, S., "Computer Program for Calculation of Complex Chemical Equilibrium Compositions and Applications. II. Users Manual and Program Description," NASA RP-1311, June 1996.

4. Gordon, S. and McBride, B. J., "Computer Program for Calculation of Complex Chemical Equilibrium Compositions, Rocket Performance, Incident and Reflected Shocks, and Chapman-Jouguet Detonations," NASA SP-273, March 1976.

5. Vincenti, W. G., and Kruger, C. H., Jr., *Introduction to Physical Gas Dynamics*, Robert E. Krieger Publishing Company, New York, 1965.

6. Hsieh, J. S., *Principles of Thermodynamics,* McGraw-Hill, New York, 1975.

7. Stull, D. R and Prophet, *JANAF Thermochemical Tables, Second Ed.*, National Bureau of Standards, NSRDS-NBS 37, June 1971.

8. Reid, R. C., Prausnitz, J. M., and Poling, B. E., *The Properties of Gases and Liquids*, Fourth Edition, McGraw-Hill, New York, 1987.

9. Bird, R .B., Stewart, W. E., and Lightfoot, E. W., *Transport Phenomena,* Wiley, New York, 1960.

10. Mani, M., Bush, R. H., and Vogel, P. G., "Implicit Equilibrium and Finite-Rate Chemistry Models for High-Speed Flow Applications," AIAA 91-3299-CP, 1991.

11. Shang, H. M., Chen, Y. S., Liaw, P., Chen, C. P., and Wang, T. S. "Investigation of Chemical Kinetics Integration Algorithms for Reacting Flows," AIAA-95-0806, 1995.

12. Drummond, J. P. "Numerical Simulation of a Supersonic Chemically Reacting Mixing Layer," D.Sc. Dissertation. George Washington University, 1988.

13. Sheun, J. S., Yoon, S., “Numerical Study of Chemically Reacting Flows Using a Lower-Upper Symmetric Successive Overrelaxation Scheme,” AIAA-88-0436, 1988.

14. Chitsomboon, T., Kumar, A., and Tiwari, S.N.,“ Numerical Study of Finite-Rate Supersonic Combustion Using Parabolized Equations,” AIAA-87-0088, 1987.

15. Hitch, B. D., Laxter, W. R., Senser, D. W., and Sojka, P. E., “On the Selection of H_2/Air Kinetic Mechanisms for Use in Supersonic Combustor Modeling,” presented at the Spring 1986 Technical Meeting of the Central States Section of the Combustion Institute, Cleveland, OH, May 1986.

16. Westbrook, C. K., “Hydrogen Oxidation Kinetics in Gaseous Detonations,” *Combustion Science and Technology*, Vol. 29, January 1982, pp. 67-81.

17. Hitch, B. D. and Senser, D.W., “Reduced H_2-O_2 Mechanisms for use in Reacting Flow Simulation,” AIAA-88-0732, 1988.

18. Tsang, W. and Hampson, R .F., “Chemical Kinetic Data Base for Combustion Chemistry. Part I. Methane/Air Combustion and Related Compounds,” *J. Phys. Chem.* Ref. Data 15, 1986, pp. 1087-1279.